Supporting Information

Exploring High-Performances anodes of Li-ion Batteries Based on the Rule of Pore-size Dependent Band Gaps in Porous Carbon Foams

Shi-Zhang Chen [a], Yuan-Xiang Deng [a], Xuan-Hao Cao [a], Wu-Xing Zhou [b*], Ye-Xin Feng [a], Li-Ming Tang [a], Ke-Qiu Chen [a*]

[a]Department of Applied Physics, School of Physics and Electronics, Hunan University, Changsha 410082, China

[b]School of Materials Science and Engineering & Hunan Provincial Key Laboratory of Advanced Materials for New Energy Storage and Conversion, Hunan University of Science and Technology, Xiangtan, 411201, China

1. STRUCTURAL INFORMATION OF CFS

1.1 Details of structures

In the MWGs, GNR stripes are rigidly interconnected by the sp^3 junctions of linear carbon chains[1] in *I*, carbon quaternion rings/tubes[2] in *II*, polyethylene carbon chain[3] in *III*, and carbon six-member rings/tubes[4] in *IV*. Inevitably, similar to γZ_S_{IV} (γ carbon foams),[4] there are still two phases of the sp^3 junctions in the FWGs and SWGs. This is because that the two edge of AGNRs may end with either half open rings (HOR) or full rings (FR) while the width of AGNRs is even *N*; Otherwise both HOR or FR are on the two edge sides, respectively. We loosely define it as *odd-even difference*. The differences between the two phases are: i) the binding pattern of sp^3 C atoms, so that the one with 90° bonding angle is energetically less favorable than the other; ii) the reduction of symmetry from odd-*N* to even-*N* CFs. For example, the AGNRs with even-*N* and ZGNRs with odd-*N* loose a twofold rotation axis C_2 and a mirror plane of symmetry σ_v. As seen in Table S1, we list the space group of all the proposed CFs.

The CFs can be rigidly built up either by unitary or compound multi-wing GNRs. In addition to the proposed $\delta\_S_{IV\&I}$ and $6612\_S_{IV\&III}$, we infer that there are many compound MWGs based CFs, for examples, structures based on *I&II, I&III, II&III, II&IV, II&III&IV*, and other MWGs.

Table S1. The space group, formation energies (E_f) normalized by the number of wings and length in the NGR

growth direction, ant the separated energies of sp^2 and sp^3 C atoms of all the proposed CFs. The column N with *odd*, *even* and *all* indicate the E_f are calculated from the *odd-N, even-N*, and *both odd-N and even-N* pore size systems, respectively.

Systems	Space Group		E_f (eV·Wing^{-1}·Å^{-1})			Energy (eV/C atoms)	
	odd	even	N	with H	without H	sp^3	sp^2
βA_S_{III}	--	P6/mmm				--	-9.09
βZ_S_{III}	P6/mmm	P6$_3$/mcm	Even	0.250178	-1.67761	-8.366	-9.242
$\delta Z\_S_{IV\&I}$	P6$_3$/mmc		All	0.262279	-1.69527	-8.579	-9.240
$6612Z\_S_{IV\&III}$	Pmmm	Pmma	Even	0.253162	-1.67462	-8.561/-8.653	-9.286/9.201
αLZ_S_{III}	Imma	Cmcm	All	0.250591	-1.70696	-8.522	-9.220
$48A\_S_{I}$	--	P4/mmm				-7.547	-9.224
$48Z\_S_{I}$	P4/mmm	I4/mcm	Odd	0.286556	-1.69331	-7.969	-9.244
$44A\_S_{II}$	P4/mmm	I4/mmm				-8.400	-9.189
$44Z\_S_{II}$	P4$_2$/mmc	Cmcm	Odd	0.127929	-1.85194	-8.405/-8.668	-9.282/-9.208
$44A\text{-}D_V$	--	P4$_2$/mmc				-8.230	-9.254
$44Z\text{-}D_V$	P4$_2$/mmc	P4/mcc	Even	0.574569	-1.35322	-8.310/-8.164	-9.276/-9.259
$44A\_D_{VI}$	I4/mmm	P4$_2$/mcm				-8.714	-9.142
$44Z\_D_{VI}$	P4$_2$/mmc	P4/mcc	Even	0.125457	-1.80233	-8.663/-8.577	-9.279/-9.210
αZ_D_{VII}	P6/mmm	P6$_3$/mmc	All	0.436899	-1.53274	-8.445	-9.206
αA_T_{VIII}	--	P6/mmm				-8.515	-9.099
αZ_T_{VIII}	P6/mmm	P63/mmc	All	0.534947	-1.43469	-8.638	-9.150

1.2 Factors that lead to the diversity of CFs

1.2.1 The edge shape and width of GNRs

CFs can be classified into zigzag and armchair CFs, but the shapes defined here are not on the edge of GNRs but perpendicular to the grow direction of the GNRs, as highlighted by the rosy sticks and balls in Fig. 1(b) in the text. This is to meet with the naming scheme of traditional CFs provided in Ref. 1. Similar to the α_S_I and γ_S_{IV}, the pore sizes are related to the width of GNRs by the numbers N, which has already been defined elsewhere,[5] the zigzag-shaped GNRs are classified by the number of dimer lines (N_z) across the ribbon width, while armchair-shaped GNRs are classified by the number of the zigzag chains (N_a) across the ribbon width. The pore shape is decided by the whether all the GNRs in the network are with the same width, since the pores are surrounded by GNRs.

1.2.2 Different width of GNRs in the CFs

When concerned about the CFs that built up by GNR stripes with different widths, as defined in

by Kuc *et al*., [1] the CFs can be distinguished to be symmetric CFs with all GNRs with the same width, while the asymmetric CFs with different width GNRs. All the CFs displayed in Fig. 1 are symmetric structures. One of the asymmetric CFs is asymmetric *48Z_S$_I$(l,m,n)*, as seen in Fig. 3(a) in the text, the TWGs building block owns three degree of freedoms of GNR width, i.e. *(l,m,n)*. For simplicity, we only consider the three quantities, even though the four outer wings are independent in this asymmetric *48Z_S$_I$(l,m,n)*. Thus, we keep the width of this four wings to be *l*, when *m=n*, the CFs with higher symmetry, as seen in Fig. 3(b); otherwise, the network is shown in Fig. 3(c), with unit cell similar to a supercell of Fig. 3(b). Nevertheless, the structures become symmetric *48_S$_I$* if *l=m=n*, and *44Z_S$_{II}$* if *m=n=2*.

1.2.3 Multilayer GNRs

Except for the single layered GNRs, the multi-layer GNRs are also attractive since the electronic properties of single layered GNRs are still maintained, and the fabrication techniques are quite mature.[6] In our work, the multi-layer GNRs are also considered in the CFs. As seen in Fig. 4(a) in text, we firstly construct the double-layer GNRs based FWGs *V* and *VI*, and TWGs *VII*, and the triple-layer GNRs based TWGs *VIII*. Than based on the multi-layer GNRs based building blocks, two 44-CFs and two α-CFs are built up, as seen in Fig. 4(b-e).

2. STABILITIES OF CFS

2.1 Energetic stabilities

2.1.1 Formation energies

We calculate the formation energies (E_f) of all the considered systems, as defined by:[4]

$$E_f = \frac{E(CFs) - n(GNR) \times E(GNR) - n(Csp^3) \times \mu(Csp^3)}{n(wing) \cdot L}, \tag{S1}$$

When the GNR is saturated with H on the two edges, and H_2 molecular energy $E(H_2)$ should be subtracted:[4]

$$E_{fH} = \frac{E(CFs) - n(GNR) \times \left[E(GNR) - n(H_2) \times E(H_2)\right] - n(Csp^3) \times \mu(Csp^3)}{n(wing) \cdot L}, \tag{S2}$$

where $E(CFs)$ is the total energy of CFs, $E(GNR)$ is the total energy of GNR. L is the length of the unit cell along the GNR growth diretions. $n(X)$ means the number of X part of the CFs. $n(H_2)$ is the

number of H atom pairs in a GNR unit. $\mu(Csp^3)$ is chemical potential of C atom in a system which is purely consist of sp^3 hybridized junctions.

The calculated formation energies of multi-wings GNRs and the designed CFs are respectively tabulated in Table S2 and Table S2.

Table S2. The formation energies of the multi-wings GNRs (MWGs) normalized by the number of wings and the length in the growth direction. The Ef *with* and *without H* indicates considering the GNRs *saturated by H* and *not saturated*, respectively.

Unit: eV/(wing·Å)	I	II	III	IV	V	VI	VII	VIII
With H	0.044	0.028	0.056	0.087	0.104	0.060	0.133	0.246
Without H	-0.601	-0.832	-0.805	-1.203	-1.617	-1.661	-1.158	-1.690

2.1.2 Binding energies

The binding energies, as given by[7]

$$E_{bind} = \left(\frac{E_{total}}{n_C} \right) - \mu_C,$$

(S3)

where E_{total} and n_C is the total energy and the total numbers of C atoms in the unit cell, respectively, and μ_C is the chemical potential of a C atom. The results are plotted in Fig. S1(a).
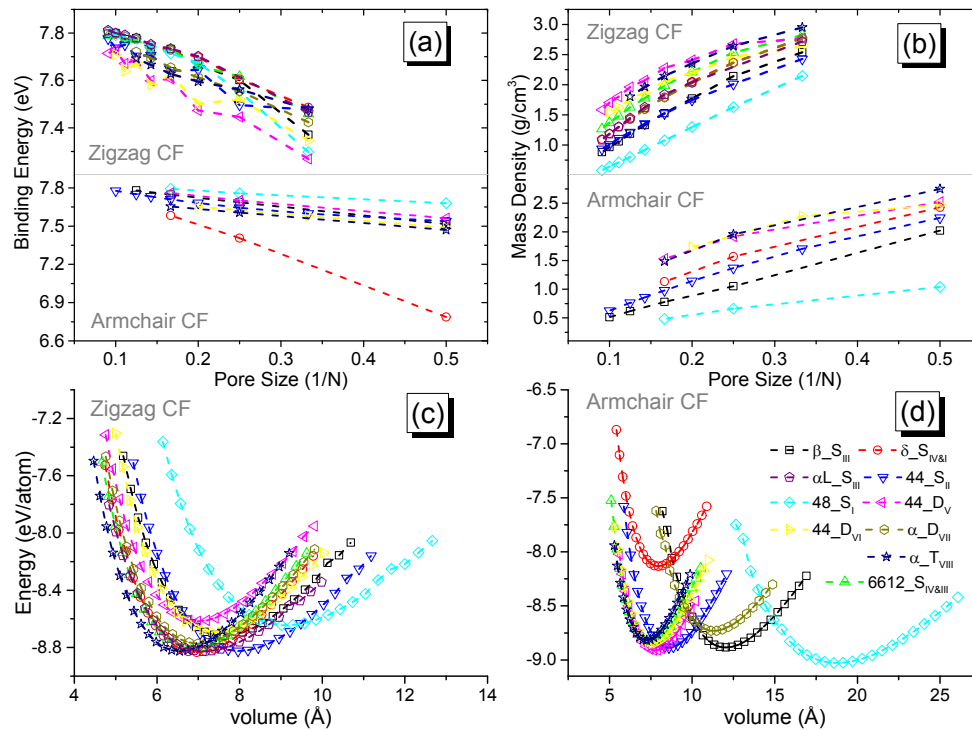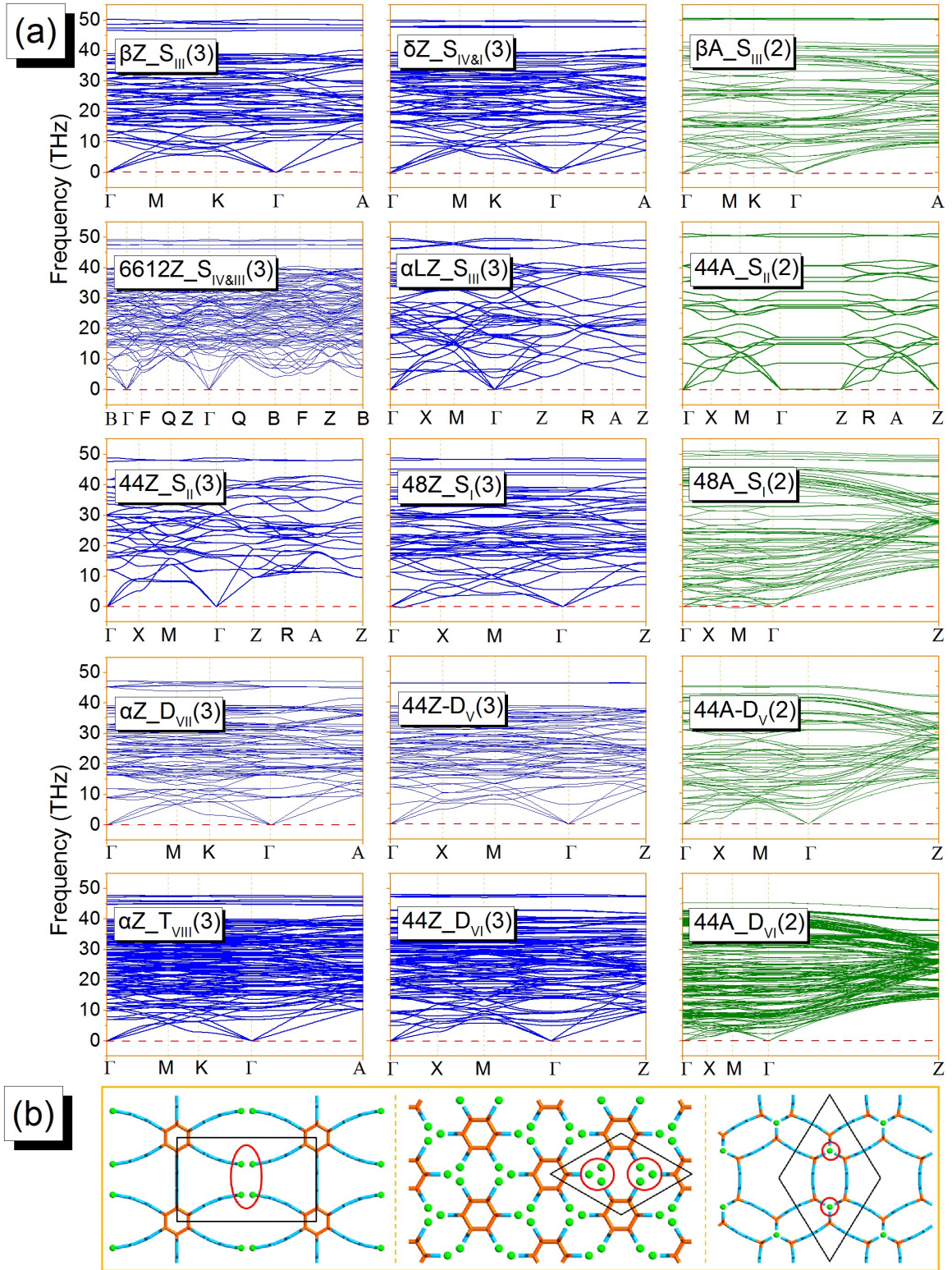
2.2 Dynamic stabilities

FIG. S2. (a)The phonon spectra of minimum pore size systems (MPSs), the blue (green) lines are for zigzag (armchair) MPSs. (b) *6612A_S$_{IV\&III}$* are not considered since the sp^3 junctions are broken large pore-size CFs. As highlighted by red circle, the *δA_S$_{IV\&I}$* and *αA_D$_{VII}$* are not stable with imaginary frequency in the phonon spectra.

This is due to the fact that, the CFs arise a junction of coplanar triatomic ring or a un-coordinated sp^2 C, as highlighted by red circles, in which the solitary electrons occupy the unhybridized p orbitals of the junction atoms and violates the octet rule.[8]

2.3 Mechanical stabilities

Table S3. The elastic constants of minimum pore size systems (MPSs), in unit of GPa.

	C_{11}	C_{22}	C_{33}	C_{44}	C_{55}	C_{66}	$C_{12}=C_{21}$	$C_{13}=C_{31}$	$C_{23}=C_{32}$
$\beta A\_S_{III}(2)$	4352.7	4347.1	5917.0	798.2	555.8	562.4	2752.3	1026.7	1020.1
$\beta Z\_S_{III}(3)$	5374.3	5372.8	9014.5	1893.7	2652.9	2652.9	1590.7	929.2	930.1
$\delta Z\_S_{IV\&I}(3)$	6442.7	6441.8	10957.9	2228.9	3370.3	3370.7	1977.2	449.7	448.8
$6612Z\_S_{IV\&III}(3)$	6005.2	7984.4	10013.9	2268.6	3809.9	2204.5	1443.2	854.9	851.7
$\alpha LZ\_S_{III}(3)$	3110.7	8885.2	11403.9	2085.4	4683.4	1753.9	1767.3	232.6	1013.8
$48A\_S_{I}(2)$	1461.1	1459.6	4872.7	17.2	1030.8	1041.2	1231.4	386.0	386.0
$48Z\_S_{I}(3)$	3678.8	3678.7	8589.8	369.2	2368.6	2369.4	1570.3	431.4	431.3
$44A\_S_{II}(2)$	5684.8	5684.8	8953.1	156.7	2255.9	2255.8	828.9	608.2	608.3
$44Z\_S_{II}(3)$	7069.3	7069.3	9913.7	463.1	2906.5	2916.0	254.9	476.1	476.0
$44A\text{-}D_{V}(2)$	6026.1	6026.1	11459.1	334.9	2710.5	2753.4	715.9	610.3	609.9
$44Z\text{-}D_{V}(3)$	5434.0	5434.4	9365.1	1548.8	2850.5	2849.6	2063.9	813.9	813.9
$44A\_D_{VI}(2)$	3854.0	3909.1	10225.3	519.8	2243.1	2383.9	707.4	626.5	616.2
$44Z\_D_{VI}(3)$	8096.5	8096.5	9613.1	741.3	2908.6	2906.9	502.8	656.7	656.6
$\alpha Z\_D_{VII}(3)$	5640.7	5627.0	11092.1	1567.4	3293.1	3298.0	2509.0	560.7	558.5
$\alpha A\_T_{VIII}(2)$	6017.0	6011.3	10494.6	1888.4	2561.5	2561.6	2234.7	512.7	518.3
$\alpha Z\_T_{VIII}(3)$	6593.6	6588.6	11626.4	2039.7	3574.2	3574.5	2524.9	407.6	406.4

By using the finite-difference scheme, the elastic constant tensors C_{ij} are obtained by deriving the total energy with strains $\epsilon_{i,j}$ as[1] $C_{ij} = \frac{\partial}{\partial \epsilon_i}\left(\frac{\partial \varepsilon}{\partial \epsilon_j}\right)$, where ε is the total energy.

The mechanical stability criteria given by[9]

$C_{44} > 0, \ C_{11} > |C_{12}|, \ (C_{11} + 2C_{12})C_{33} > 2C_{13}^2$ for hexagonal systems;

$C_{11} > 0, \ C_{33} > 0, \ C_{44} > 0, \ C_{66} > 0, \ (C_{11} - C_{12}) > 0, \ (C_{11} + C_{33} - 2C_{13}) > 0, \ [2(C_{11} + C_{12}) + C_{33} + 4C_{13}] > 0$ for tetragonal systems;

$C_{11} > 0, \ C_{22} > 0, \ C_{33} > 0, \ C_{44} > 0, \ C_{55} > 0, \ C_{66} > 0, \ (C_{11} + C_{22} - 2C_{12}) > 0, \ (C_{11} + C_{33} - 2C_{13}) > 0, \ (C_{22} + C_{33} - 2C_{23}) > 0, \ [C_{11} + C_{12} + C_{33} + 2(C_{12} + C_{13} + C_{23})] > 0$ for orthorhombic systems.

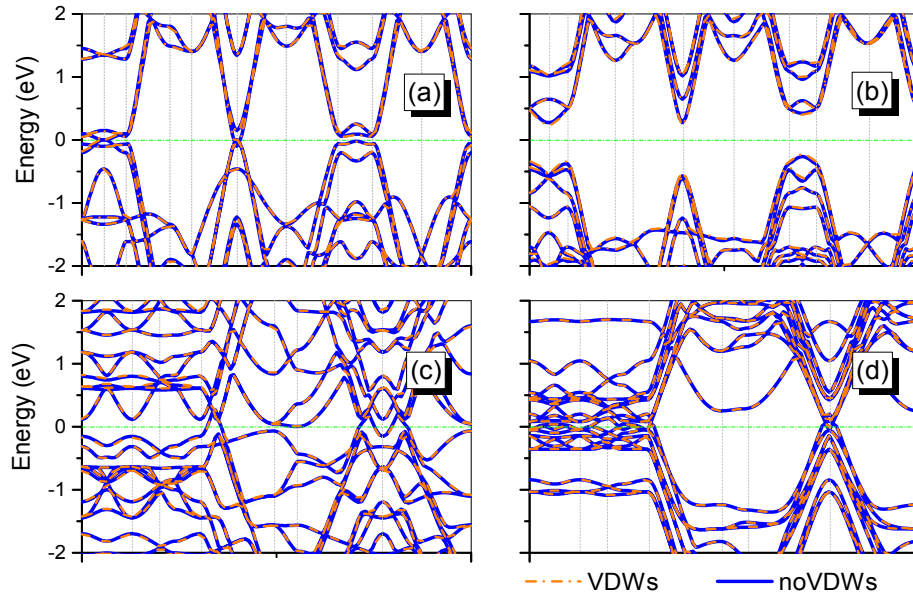3. THE INFLUENCE OF VAN DER WAALS INTERACTION AND THE STACKING IN THE MULTILAYER CFS.

FIG. S3. The band structures of (a) *44Z_D$_V$(5)*, (b) *44Z_D$_{VI}$(5)*, (c) *αZ_D$_{VII}$(5)* and (d) *αZ_T$_{VIII}$(5)*. The blue lines and red dash lines indicate the band structures gained from considering *with* and *without* van der Waals interactions, respectively.

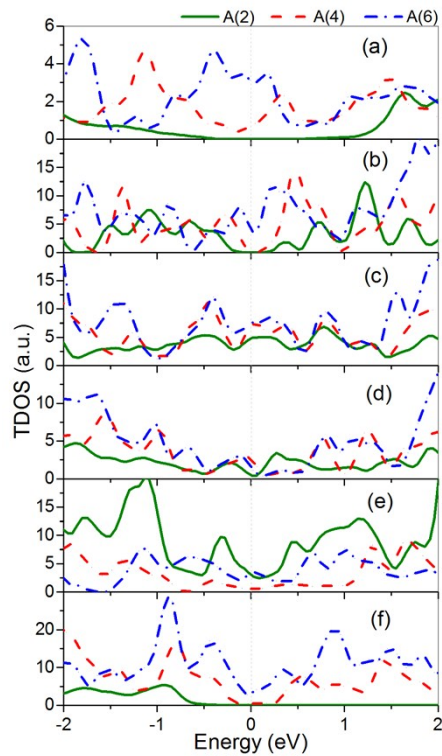4. THE INFLUENCE OF SPIN POLARIZATIONS ON THE BAND STRUCTURES ARMCHAIR CFS.

FIG. S4. The total density of states (TDOS) of armchair (a) $44A\_S_{II}$, (b) $48A\_S_I$, (c) βA_S_{III}, (d) $44A\_D_V$, (e) $44A\_D_{VI}$, and (f) αA_T_{VIII} CFs. The gray dot line indicates the Fermi level.
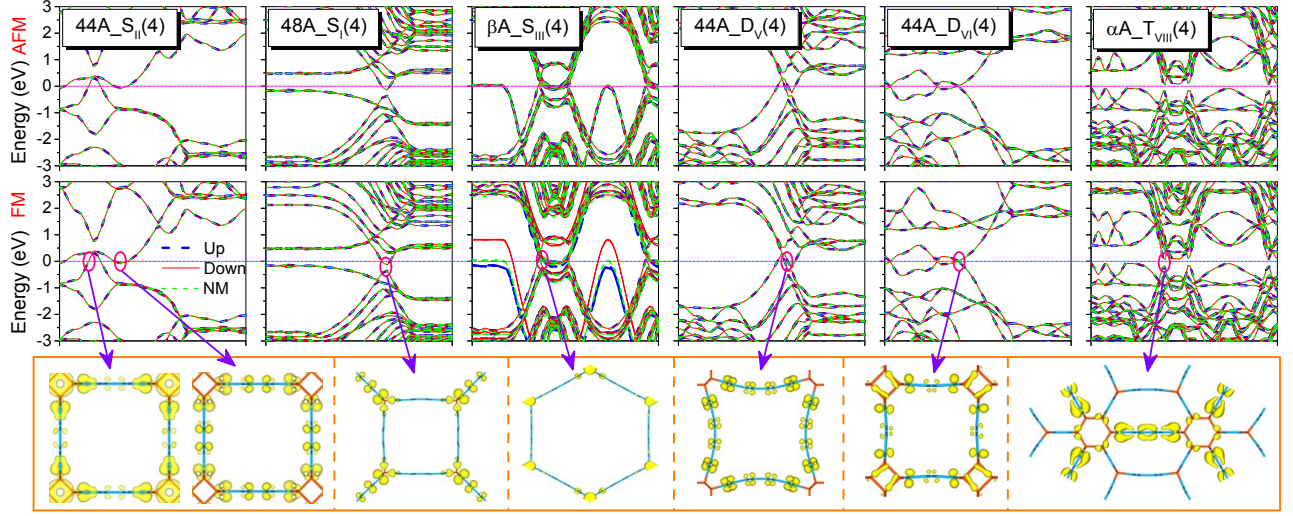

FIG. S5. The band structures and the partial charge density distributions of $44A\_S_{II}$, $48A\_S_I$, βA_S_{III}, $44A\_D_V$, $44A\_D_{VI}$, and αA_T_{VIII} from left to right, with the pore size $N=4$. The upper (bottom) row of band structures are calculated under anti-ferromagnetism (ferromagnetism) state, in which the blue dash (red) lines indicate the bands of up spin (down spin) electrons. The green dash lines are gained from spin unpolarized calculations. The partial charge density are calculated at where bands cross Fermi level, as highlighted by magenta circles and purple arrows.

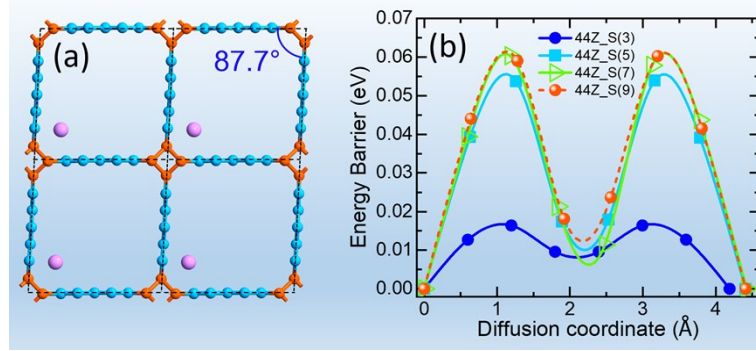5. THE LIBS PERFORMANCES USING CFS AS ANODE MATERIALS

FIG. S6. (a) Structure of $44Z\_S_{II}(7)$ with Li^+ inserting at the corner. The lithiation at the corner will reduce the symmetry. (b) The diffusion energy barriers of Li^+ in $44Z\_S_{II}(3)$, $44Z\_S_{II}(5)$, $44Z\_S_{II}(7)$, and $44Z\_S_{II}(9)$.

Table S4. Comparisons of charge transfer from Li to $44Z\_S_{II}$ networks. In unit of elementary charge.

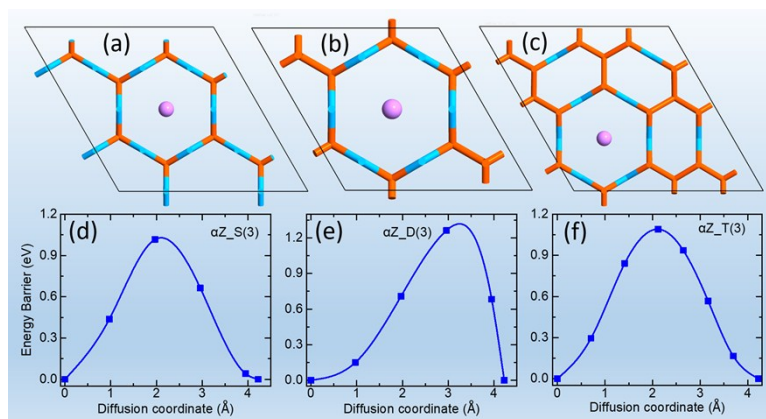|	$44Z\_S_{II}(3)$	$44Z\_S_{II}(5)$	$44Z\_S_{II}(7)$	$44Z\_S_{II}(9)$
Li^+ at pore center	0.889	0.523	0.236	0.099
Li^+ at pore corner	0.911	0.910	0.909	0.909

FIG. S7. Li$^+$ diffuses along pore center of α-CFs. (a-c) the schematic structures of $\alpha Z\_S_I(3)$, $\alpha Z\_D_{VII}(3)$, and $\alpha Z\_T_{VIII}(3)$ with Li atom sites in pore center. (d-f) the correcponding diffusion energy barriers of Li$^+$.

References

1. A. Kuc and G. Seifert, *Phys. Rev. B*, 2006, **74**, 214104.

2. Z. Zhao, B. Xu, L.-M. Wang, X.-F. Zhou, J. He, Z. Liu, H.-T. Wang and Y. Tian, *ACS Nano*, 2011, **5**, 7226-7234.

3. X. Jiang, J. Zhao, Y. L. Li and R. Ahuja, *Adv. Funct. Mater.*, 2013, **23**, 5846-5853.

4. S.-Z. Chen, W.-X. Zhou, J.-F. Yu and K.-Q. Chen, *Carbon*, 2017.

5. Y.-W. Son, M. L. Cohen and S. G. Louie, *Phys. Rev. Lett.*, 2006, **97**, 216803.

6. B. Sahu, H. Min and S. K. Banerjee, *Phys. Rev. B*, 2010, **82**, 115426.

7. S.-Z. Chen, F. Xie, F. Ning, Y.-Y. Liu, W.-X. Zhou, J.-F. Yu and K.-Q. Chen, *Carbon*, 2017, **111**, 867-877.

8. Z. G. Fthenakis, *RSC Adv.*, 2017, **7**, 9790-9794.

9. Z.-j. Wu, E.-j. Zhao, H.-p. Xiang, X.-f. Hao, X.-j. Liu and J. Meng, *Phys. Rev. B*, 2007, **76**, 054115.